The influence of line tension on the formation of liquid bridges in atomic force microscope-like geometry



2007 J. Phys.: Condens. Matter 19 466104

(http://iopscience.iop.org/0953-8984/19/46/466104)

IOP PUBLISHING JOURNAL OF PHYSICS: CONDENSED MATTER

J. Phys.: Condens. Matter **19** (2007) 466104 (13pp) doi:10.1088/0953-8984/19/46/466104

# The influence of line tension on the formation of liquid bridges in atomic force microscope-like geometry

**F Dutka and M Napiórkowski**

Instytut Fizyki Teoretycznej, Uniwersytet Warszawski, 00-681 Warszawa, Hoża 69, Poland

E-mail: fdutka@fuw.edu.pl

Received 3 July 2007, in final form 12 September 2007
Published 10 October 2007
Online at stacks.iop.org/JPhysCM/19/466104

**Abstract**

We investigate thermodynamic and geometrical conditions for the formation of a liquid bridge between a planar and conical walls modeling atomic force microscope (AFM). Our macroscopic analysis is based on the grand canonical functional of the shape of the liquid–vapor interface which contains the relevant bulk, surface and line free energies. The phase diagram of such a confined fluid displays the existence of two phases: one with a liquid bridge connecting the walls, and the other without a bridge. The structure of the corresponding coexistence line is determined and its dependence on the value of the line tension coefficient is discussed.

## 1. Introduction

The behavior of fluids confined in nanosized structures depends sensitively on the properties of the enclosing walls [1, 2]. The equilibrium paradigm of such an influence is provided by the capillary condensation phenomenon in a slit. Despite thermodynamic conditions favoring the gas phase in the bulk, the liquid phase may fill the space between the slit walls [3–7]. The shift of the gas–liquid coexistence line $\mu = \mu_{\mathrm{h}}(T)$ in the slit of width $h$ with respect to its position in the bulk system $\mu = \mu_0(T)$ is described by the Kelvin law: $\mu_0(T) - \mu_{\mathrm{h}}(T) \propto 1/h$ [8].

When the walls confining the fluid are non-planar and resemble the AFM geometry then one may expect the formation of a liquid bridge linking the opposite walls [9–15] at thermodynamic conditions that favor the gas phase in the bulk. The size and the shape of the liquid bridge depend on the system's geometry as well as on the thermodynamic state specified by the chemical potential $\mu$ and temperature $T$; the range in which these parameters can vary is one of the objects of our analysis. The presence of a liquid bridge induces an additional force—with respect to the situation without a bridge—acting between the walls; this force must be taken into account when analyzing the atomic force microscope measurements [16–20]. The formation of the liquid bridge is also exploited in dip-pen nanolithography [21–24]. There the existence of the bridge enables the flow of a particular type of molecule from the tip of the AFM onto the planar substrate. The size of the patterns that are produced depends on the geometry

  

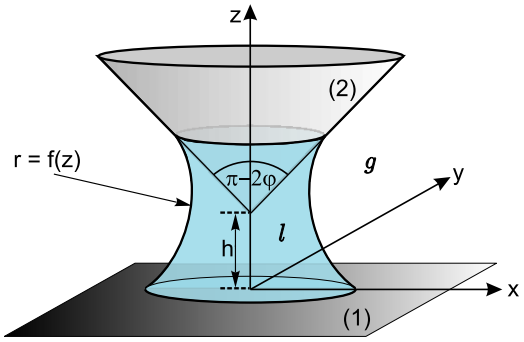


**Figure 1.** A liquid-like bridge (l) surrounded by the gas phase (g) connects the planar substrate (1) and the AFM tip of the conical shape (2).

(This figure is in colour only in the electronic version)

of the bridge, which itself is controlled by the thermodynamic state of the system and its walls' geometry. These two examples already show that the knowledge of precise thermodynamic and geometrical conditions for the existence of liquid bridges together with their morphological properties is of crucial importance.

In this paper we investigate the morphological phase transitions taking place in a three-dimensional (3D) fluid confined by the walls resembling the AFM geometry. They consist of a planar substrate and the surface of a cone modeling the cantilever's tip. Our study is based on a macroscopic approach in the grand canonical ensemble with the purpose of constructing the relevant phase diagram and determining the possible shapes of the liquid-like bridge spanned between the planar substrate and the conical tip. In particular, we discuss the influence of the line tension on the structure of the coexistence curve and examine the special cases which turn out to be related to the filling transition.

## 2. Shape of meniscus

We consider fluid confined between two inert substrates; see figure 1. The surface of the lower substrate denoted by (1) is an infinite plane $z = 0$ and the upper substrate denoted by (2) forms an infinite cone characterized by the opening angle $\pi - 2\varphi$. The distance between the cone's apex and the plane $z = 0$ is denoted by $h$; the parameters $h$ and $\varphi$ completely characterize the system's geometry which has cylindrical symmetry. In cylindrical coordinates the cone is described by equation $r = a(z) = (z - h)\cot\varphi$, where $r = \sqrt{x^2 + y^2}$ and $z > h$. The system under study resembles the AFM-like geometry in which the conical substrate (2) plays the role of the microscope's tip. In the limit $\varphi = 0$, $h \neq 0$, the geometry becomes that of a slit with two parallel walls separated by the distance $h$. In another limiting case corresponding to $\varphi \neq 0$ and $h = 0$, the confining walls can be obtained by rotating a two-dimensional wedge with the opening angle $\varphi$ around the axis perpendicular to one of the walls and intersecting the wedge's apex. The interesting point about such a confining geometry is that it might allow—under appropriate thermodynamic conditions—for a filling transition [25, 26]. Thermodynamic states of the fluid are specified by the temperature $T$ and chemical potential $\mu$, and are assumed to be located away from the bulk liquid–gas critical point.

Our macroscopic analysis is based on the grand canonical functional $\Omega([f], T, \mu, h, \varphi)$ which is a functional of the interfacial shape $f$ and is parametrized by the fluid thermodynamic

state $T$, $\mu$ and geometric parameters $h$, $\varphi$. The functional $\Omega$ is constructed such that it contains all the relevant bulk, surface and line contributions to the constrained grand canonical free energy correspondingly to a given interfacial shape $f$ [8]. The allowed shapes of the liquid–gas interface are assumed to be cylindrically symmetric, i.e. $r = f(z)$. The equilibrium shape $\bar{f}(z; T, \mu, h, \varphi)$ minimizes the functional $\Omega$ and leads to the thermodynamic grand canonical potential $\bar{\Omega}(T, \mu, h, \varphi) = \Omega([\bar{f}(z; T, \mu, h, \varphi)], T, \mu, h, \varphi)$. To shorten notation we shall refrain from displaying the dependence of analyzed functions and functionals on parameters $T$, $\mu$, $h$, $\varphi$ from now on. Comparison of the grand canonical potential values corresponding to configurations with and without the bridge allows us to tell which configuration is favorable under given thermodynamic and geometric conditions, and to construct the relevant phase diagram. In what follows we shall work with the functional $\Delta\Omega[f]$ representing the difference between the grand potential corresponding to the state with a bridge and without it. For practical reasons we change the parametrization, and instead of temperature $T$ we switch to angles $\theta_i$, $i = 1, 2$, related to the temperature-dependent surface tension coefficients $\sigma_{ig}$, $\sigma_{il}$, and $\sigma_{lg}$, $i = 1, 2$ via the Young equation [8]

$$\sigma_{ig} - \sigma_{il} = \sigma_{lg} \cos\theta_i, \qquad i = 1, 2. \tag{1}$$

In the above equation, $\sigma_{lg}$ denotes the liquid–gas surface tension while $i$ stands for the $i$th substrate and—for example—$\sigma_{1l}$ denotes the substrate 1–liquid surface tension. In what follows, the above relation will be applied also to thermodynamic states slightly off the bulk coexistence.

The present analysis—contrary to the two-dimensional version of the problem [27]—also takes into account the linear contributions to the free energy which are related to the three phase contact lines where gas, liquid and the $i$th substrate meet. The line tension coefficient which measures the corresponding free energy per unit length of the three phase contact line is denoted by $\tau_{ilg}$. In the present approach these coefficients are considered as given. However, in a more refined version of the present analysis based on the effective capillary Hamiltonian approach one could make an attempt to determine these coefficients by calculating the total free energy of the inhomogeneous system and then extracting the relevant linear contributions. This approach is left for future studies.

In the present macroscopic analysis the functional $\Delta\Omega[f]$ has the following form:

$$\begin{aligned}\Delta\Omega[f] = {} & V(\mu_0 - \mu)(\rho_l - \rho_g) + A_{lg}\sigma_{lg} + A_1(\sigma_{1l} - \sigma_{1g}) + A_2(\sigma_{2l} - \sigma_{2g}) \\ & + L_{1lg}\tau_{1lg} + L_{2lg}\tau_{2lg}\end{aligned} \tag{2}$$

where $V$ denotes the liquid bridge's volume, $A_{lg}$, $A_1$, $A_2$ are the areas of the liquid–gas, substrate 1–liquid, and substrate 2–liquid interfaces, $L_{1lg}$, $L_{2lg}$ are the lengths of the three phase contact lines, and $\Delta\rho = \rho_l - \rho_g > 0$ is the liquid and gas number density difference.

After representing the volume of the liquid bridge, its surfaces, and the lengths of the three phase contact lines by appropriate integrals, the grand canonical functional takes the following form:

$$\begin{aligned}\frac{\Delta\Omega[f]}{2\pi\sigma_{lg}} = {} & \int \mathrm{d}z \left[ f(z)\sqrt{1 + \left(\frac{\mathrm{d}f}{\mathrm{d}z}\right)^2} + \frac{f(z)^2 - a(z)^2\Theta(z-h)}{2\lambda} \right] \\ & \times \Theta\Big(f(z)\Big)\,\Theta\Big(f(z) - a(z)\Big)\Theta(z) \\ & + \int \mathrm{d}z \left[ -\cos\theta_1 \frac{f(z)^2}{2}\delta(z) - \frac{\cos\theta_2}{\sin\varphi}\, a(z)\,\Theta(z-h)\,\Theta\Big(f(z) - a(z)\Big) \right] \\ & + \int \mathrm{d}z\, [\tilde{\tau}_{1lg} f(z)\delta(z) + \tilde{\tau}_{2lg}\cot\varphi\,\Theta(z-h)\,\Theta(f-a)],\end{aligned} \tag{3}$$

where $\lambda = \sigma_{lg}/\Delta\mu\Delta\rho$, $\Delta\mu = \mu_0 - \mu \geqslant 0$, and $\tilde{\tau}_{ilg} = \tau_{ilg}/\sigma_{lg}$. The parameters $\lambda$ and $\tilde{\tau}_{ilg}$ have the dimension of length. The symbols $\Theta(z)$ and $\delta(z)$ denote the Heaviside and Dirac functions, respectively.

The equilibrium interfacial shape $\bar{f}(z)$ minimizes $\Delta\Omega[f]$ and fulfills the equation

$$\frac{1}{\bar{f}(z)\sqrt{1+\bar{f}'(z)^2}} - \frac{\mathrm{d}}{\mathrm{d}z}\frac{\bar{f}'(z)}{\sqrt{1+\bar{f}'(z)^2}} = -\frac{1}{\lambda} \tag{4}$$

supplemented by two boundary conditions,

$$\begin{aligned} 0 &= \left[\cos\theta_1 + \frac{\bar{f}'(z)}{\sqrt{1+\bar{f}'(z)^2}} - \frac{\tilde{\tau}_{1lg}}{\bar{f}(z)}\right]\Bigg|_{z=0} \\ 0 &= \left[\cos\theta_2 - \frac{\sin\varphi + \cos\varphi\,\bar{f}'(z)}{\sqrt{1+\bar{f}'(z)^2}} - \frac{\tilde{\tau}_{2lg}}{\bar{f}(z)}\cos\varphi\right]\Bigg|_{z=z_2}, \end{aligned} \tag{5}$$

where the coordinate $z_2$ is such that $\bar{f}(z_2) = a(z_2)$. Both the equation for the interfacial profile (4) and the boundary equations (5) follow from the minimization of $\Delta\Omega[f]$. The left-hand side (lhs) of (4) is equal to the mean curvature of the interface [28] and thus the surface of the bridge has constant and negative mean curvature; it is called a concave nodoid [29, 30].

Note that after introducing the contact angles $\gamma_1$ and $\gamma_2$ (see figure 2)

$$\left.\frac{\mathrm{d}\bar{f}}{\mathrm{d}z}\right|_{z=0} = -\frac{1}{\tan\gamma_1} \tag{6}$$

$$\left.\frac{\mathrm{d}\bar{f}}{\mathrm{d}z}\right|_{z=z_2} = \frac{1}{\tan(\gamma_2+\varphi)} \tag{7}$$

the boundary equations (5) take the form of modified Young equations [31]:

$$\cos\gamma_1 = \cos\theta_1 - \frac{\tilde{\tau}_{1lg}}{\bar{f}(0)} \tag{8}$$

$$\cos\gamma_2 = \cos\theta_2 - \cos\varphi\,\frac{\tilde{\tau}_{2lg}}{\bar{f}(z_2)}. \tag{9}$$

In the case of vanishing line tension coefficients, i.e. $\tau_{ilg} = 0, i = 1, 2$, the contact angles $\gamma_i$ become equal to the angles $\theta_i$ present in the Young equation, (1). Unfortunately (4) supplemented by the above boundary conditions, (5), cannot be solved analytically[1]. One has to resort to numerical procedures for solving the second-order differential equation (4) on a segment $0 \leqslant z \leqslant z_2$ for which boundary conditions (5) specified at both ends of the segment must be fulfilled. In these circumstances we choose the shooting method [32] as the most appropriate for such problems. For a given starting point $z_2 > h$, one calculates the quantities $\bar{f}(z_2) = a(z_2)$ and $\bar{f}'(z_2)$ in accordance with the boundary conditions, (9),

[1] After the change of variables $u(\bar{f}) = \frac{\mathrm{d}\bar{f}}{\mathrm{d}z}(\bar{f})$, (4) takes the following form:

$$\frac{\mathrm{d}u^2}{\mathrm{d}\bar{f}} = \frac{2}{\lambda}(1+u^2)^{3/2} + \frac{2}{\bar{f}}(1+u^2) \tag{10}$$

and can be rewritten as

$$\int \mathrm{d}\bar{f}\, z(\bar{f}) = \pm\int \frac{\bar{f}^2 - 2C}{\sqrt{(2\lambda\bar{f})^2 - (\bar{f}^2-2C)^2}}\mathrm{d}\bar{f} \tag{11}$$

where $C$ is the integration constant. The elliptical integral on the right-hand side (rhs) cannot be calculated analytically. The function $\bar{f}(z)$ cannot be presented in algebraic form as for the two-dimensional problem [27].

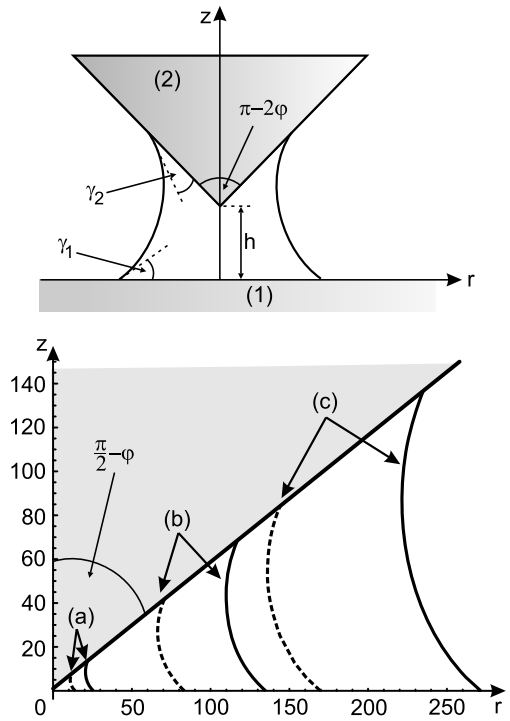


**Figure 2.** The cross section of the system with the liquid bridge present (upper diagram) and the shapes (of the right-hand halves) of the liquid bridges (lower diagram) (dashed lines) for a specific choice of parameters $\varphi = \pi/6$, $\theta_1 = \theta_2 = \pi/6$, $\tilde{\tau}_{1lg} = \tilde{\tau}_{2lg} = 0$, and (a) $\lambda = 10h$, (b) $\lambda = 50h$, (c) $\lambda = 100h$. The variables $r$ and $z$ are displayed in $h$ units. For comparison we show the shapes of liquid bridges obtained in the two-dimensional case (solid lines) for the same choice of the above parameters.

and then the function $\bar{f}(z)$ is constructed on the segment $[0, z_2]$ by solving (4). Once the point $z = 0$ is reached, the boundary condition in (8) is checked. If it is fulfilled, then the constructed function is accepted as $\bar{f}(z)$ (see figure 2). If it is not, then the whole procedure must be repeated for a new choice of the starting point $z_2$; in the case when the angle $\gamma_1$ calculated from (6) is larger than that obtained from (8) one increases $z_2$, while in the opposite case one starts with a decreased value of $z_2$. The existence of the solution of (4) depends on the choice of the thermodynamic state and the values of the geometric parameters. If there is no solution $\bar{f}(z)$ to (4) then the stable phase of our system corresponds to the absence of a liquid bridge. Figure 2 shows interfacial shapes (broken lines) in the case of identical substrates, fixed distance $h$, zero line tension coefficients, and three different choices of angle $\varphi$; for comparison, the corresponding shapes obtained in the two-dimensional case [27] for the same choice of geometric and thermodynamic parameters are plotted (solid lines). This comparison makes sense when $\tilde{\tau}_{1lg} = \tilde{\tau}_{2lg} = 0$ which is the case. We note that—for the given choice of thermodynamic parameters—the two-dimensional bridges are broader than the three-dimensional ones.

## 3. Phase diagrams

Once the equilibrium shape $\bar{f}(z)$ of the liquid bridge is determined, one can evaluate the corresponding grand canonical free energy $\Delta\Omega[\bar{f}]$ relative to a configuration without the

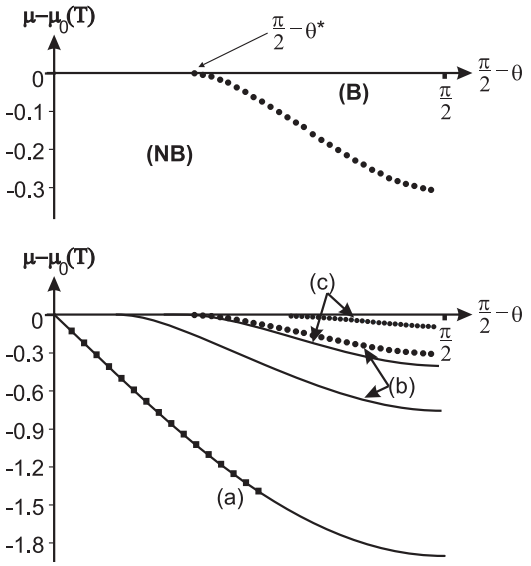


**Figure 3.** The schematic phase diagrams in variables $\mu - \mu_0(T)$ (measured in $\sigma_{lg}/h\Delta\rho$ units) and $\pi/2 - \theta$ displaying the coexistence lines of phases in which the liquid bridge is present (B) and absent (NB) for the case of identical substrates ($\theta_1 = \theta_2 = \theta$) and vanishing line tension coefficients ($\tilde{\tau}_{1lg} = \tilde{\tau}_{2lg} = 0$). The upper diagram corresponds to $\varphi = \pi/6$; the lower diagram displays the coexistence lines in a three-dimensional system (dotted lines) and—for comparison—in two-dimensional systems (solid lines) for different values of the angle $\varphi$: (a) $\varphi = 0$, (b) $\varphi = \pi/6$, (c) $\varphi = \pi/4$.

bridge. Depending on the sign of $\Delta\Omega[\bar{f}]$, three cases are possible: (a) $\Delta\Omega[\bar{f}] < 0$—the bridge phase is favorable; (b) $\Delta\Omega[\bar{f}] > 0$—the phase without the bridge is favorable; (c) $\Delta\Omega[\bar{f}] = 0$—two previous phases coexist along a line in the $(T, \mu)$-plane which will be denoted as $\mu = \mu_{AFM}(T)$. The coexistence line $\mu = \mu_{AFM}(T)$ depends, in addition to temperature $T$, also on the geometrical parameters $h, \varphi$.

Before presenting the results for the currently studied three-dimensional case, we recall that a similar analysis performed for the two-dimensional case showed that both the Kelvin law for capillary condensation in a slit of width $h$ and the complete filling transition in an infinite wedge (characterized by the opening angle $\varphi$) can be treated as special cases of bridge formation [27]. In particular, the lowest temperature at which the bridge can be formed (for a given angle $\varphi$) coincides with the wedge filling temperature $T_f(\varphi)$ such that $\theta(T_f(\varphi)) = \pi/2 - \varphi/2$. The wedge filling temperature is an increasing function of $\varphi$ [25, 26]. Note that the geometry of the two-dimensional system under present consideration constrains the range of angle $\varphi$ to $[0, \pi/2]$; if the filling transition were considered for wedges with the opening angle $\varphi$ from the range $[0, \pi]$ ($\varphi = \pi$ corresponding to a planar substrate) then $T_f(\pi) = T_w$, where $T_w$ denotes the wetting temperature. Upon crossing the coexistence curve at a fixed value of angle $\theta$ towards larger values of the chemical potential $\mu$, the system exhibits discontinuous phase transition at which a bridge with a circular liquid–gas interface is formed. The width of the bridge is inversely proportional to $\Delta\mu$ and additionally depends on the opening angle $\varphi$ and height $h$. It becomes infinite for parallel walls, i.e. for $\varphi = 0$. The dependence of the phase diagram on the parameters $h$ and $\Delta\mu$ enters via the product $h\Delta\mu$.

The phase diagrams obtained for the three-dimensional system in the case of vanishing line tensions, i.e. for $\tilde{\tau}_{1lg} = \tilde{\tau}_{2lg} = 0$, do not differ qualitatively from those in two dimensions;

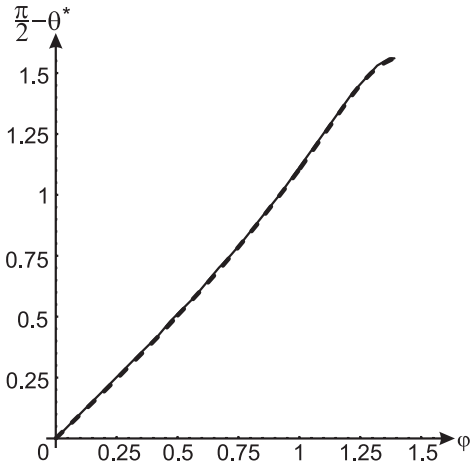


**Figure 4.** The value of angle $\pi/2 - \theta^*$ at which the filling transition takes place as a function of angle $\varphi$. The dashed line represents the results of numerical analysis described in the text for the case $\tilde{\tau}_{1lg} = \tilde{\tau}_{2lg} = 0$, $h = 0$; the solid line is obtained under the assumption that the liquid bridge's surface is described by a catenoid.

see figure 3. Both for two and three dimensions the coexistence line $\mu_{AFM}$ is a decreasing function of the angle $\pi/2-\theta$. Obviously, the coexistence lines in two and three dimensions are identical in the special case of a slit of width $h$ corresponding to the limit $\varphi = 0$. Similarly, as in two dimensions, the filling transition temperature $T_f(\varphi)$ plays a distinguished role; the AFM coexistence lines meet the bulk coexistence tangentially at the value of the parameter $\pi/2 - \theta$ corresponding to the filling temperature $T_f(\varphi)$. In the present three-dimensional case the filling transition takes place in the AFM geometry with $h = 0$. This particular value of parameter $\pi/2 - \theta$ is denoted as $\pi/2 - \theta^*$, where $\theta^* = \theta(T_f(\varphi))$. At this point ($\pi/2 - \theta^*$, $\Delta\mu = 0$) the liquid bridge has zero mean curvature (see (4)) and therefore the 'shape' of a catenoid. Figure 4 presents the numerically obtained plot of $\pi/2-\theta^*$ as a function of angle $\varphi$. Note that for small $\varphi$-values the angle $\pi/2-\theta^*$ depends linearly on $\varphi$, i.e. $\theta^* = \pi/2-\varphi$. This last relation differs from the two-dimensional case where one has $\theta^* = \pi/2 - \varphi/2$; see [25]. It is worthwhile noting that the value $\theta^* = 0$ is reached for $\varphi = \varphi_0 < \pi/2$, where $\varphi_0 = 1.42$. Technically, $\varphi_0$ presents the largest value of angle $\varphi$ for which inscribing a catenoid (corresponding to angle $\theta = \theta^*$) into AFM geometry is possible.

The above results were obtained within macroscopic analysis which does not take into account the interaction between the liquid–gas interface and the substrates explicitly, as specified for example by the interface potential $\omega(f)$ [33, 34]. We note that the formulation of this problem on the mesoscopic scale—in which the interface potential plays an important role—meets from the very outset some basic questions related to the structure of the effective Hamiltonian relevant for the present geometry in which the substrate's curvature varies along the AFM tip. One possible way of dealing with these problems is to start the analysis from the microscopic level as specified, for example, by density functional theory [35–38].

## 4. The role of line tension

In order to determine the influence of line tension on the structure of a phase diagram, one must know the line tension coefficient's dependence on the thermodynamic state of the system within the range of interest here, say for temperatures between the wetting temperature and the

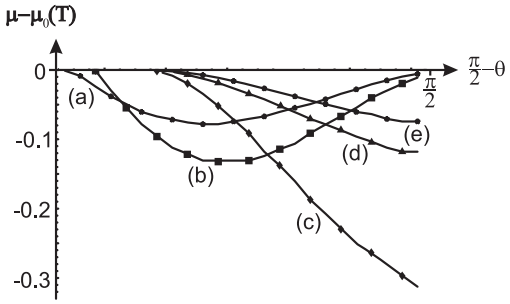


**Figure 5.** Numerically determined coexistence lines corresponding to different values of line tension: (a) $\tilde{\tau}_{1lg} = \tilde{\tau}_{2lg} = -2h$, (b) $\tilde{\tau}_{1lg} = \tilde{\tau}_{2lg} = -h$, (c) $\tilde{\tau}_{1lg} = \tilde{\tau}_{2lg} = 0$, (d) $\tilde{\tau}_{1lg} = \tilde{\tau}_{2lg} = h$, (e) $\tilde{\tau}_{1lg} = \tilde{\tau}_{2lg} = 2h$ for specific choice of $\varphi = \pi/6$. The variable $\mu - \mu_0(T)$ is measured in $\sigma_{lg}/h\Delta\rho$ units. Solid lines are drawn to guide the eye.

temperature of capillary condensation. In spite of a rather vast literature on this subject [39–43] there is still a lack of general statements applicable outside the immediate vicinity of the wetting points where universal behavior is observed. We recall that the line tension coefficient $\tau_{ilg}$ can be of either sign and its value changes significantly in the vicinity of the wetting temperature $T_{wi}$, i.e. the temperature at which the angle $\theta_i$ vanishes, $\theta_i(T_{wi}) = 0$, [44–46]. The behavior of the line tension coefficient near $T_{wi}$ depends on the order of the wetting transition and on the type of interaction between particles constituting the system. The universal property of this dependence is that the line tension coefficient is an increasing function for $T \nearrow T_{wi}$, and the limiting value $\tau_{ilg}(T_{wi})$ is positive for the first-order wetting (and can even be infinite for a specific choice of interactions), and is zero for critical wetting [44].

In view of the lack of precise information on the dependence of line tension coefficients on the chemical potential and temperature, we shall estimate their influence on the phase diagram in the simplest model by assuming $\tau_{ilg}$ to be constant parameters. We shall examine the system properties corresponding to different constant values and, in particular, both signs will be taken into account. For simplicity, in the following analysis we again consider identical substrates, i.e. $\theta_1 = \theta_2 = \theta$ and $\tilde{\tau}_{1lg} = \tilde{\tau}_{2lg} = \tilde{\tau}$.

The line tension influences the grand canonical potential not only through its presence in (3) but also via boundary conditions where it affects the contact angles, (8), (9). The coexistence lines corresponding to different values of the line tension are shown on figure 5. For positive $\tau$-values the shape of the coexistence line does not change qualitatively with respect to the $\tau = 0$ case; it is still monotonic, i.e. $\mu_{AFM}$ is an increasing function of $\theta$ and achieves the lowest value at the wetting temperature where $\theta(T = T_w) = 0$.

On the other hand, for $\tau < 0$ the coexistence lines are not monotonic; they exhibit a local minimum and approach the bulk coexistence line $\mu = \mu_0$ for $T \to T_w$; see figure 5. One can argue for this type of behavior at small $\theta$ values in the following way based on (8), (9): close to the wetting temperature both $\bar{f}(z_2)$ and $\bar{f}(0)$ must increase in order to prevent the rhs of (8), (9) from exceeding 1. Thus the size of the bridge which is proportional to the $(\mu_0 - \mu)^{-1}$ also increases, which means that $\mu_{AFM}$ approaches $\mu_0$.

The presence of line tension also influences the temperature at which the coexistence lines approach (tangentially) the bulk coexistence. For positive line tensions this particular temperature does not depend on the actual $\tau$-value. For negative line tensions this temperature decreases with $|\tau|$. This behavior is illustrated in figures 6 and 7.

For two-dimensional systems [27] and for three-dimensional systems with $\tau = 0$ there is only one quantity with the dimension of length which can be built out of the system parameters,

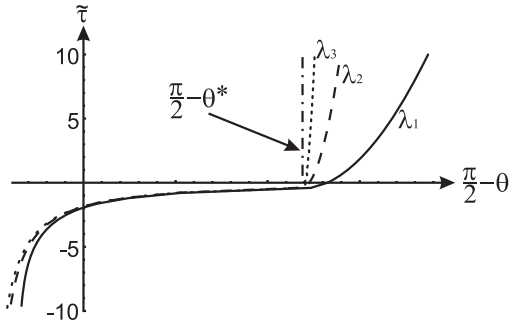


**Figure 6.** The value of parameter $\tilde{\tau} = \tau/\sigma_{lg}$ (measured in $h$ units) as a function of angle $\pi/2 - \theta$ at which the corresponding coexistence line on the phase diagram intersects the line (a) $\lambda = \lambda_1 = 10^3 h$ (solid line), (b) $\lambda = \lambda_2 = 10^4 h$ (dashed line), (c) $\lambda = \lambda_3 = 10^5 h$ (dotted line). For $\lambda = \infty$ ($\mu = \mu_0$) the resulting plot becomes vertical at $\pi/2 - \theta^*$ for positive $\tilde{\tau}$ (dashed–dotted line). The opening angle is fixed at $\varphi = \pi/6$.

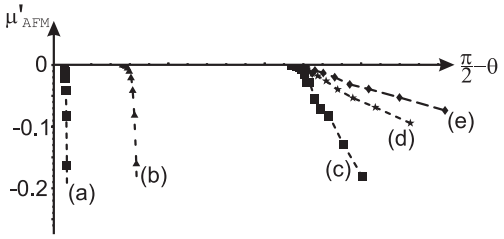


**Figure 7.** Plots of numerically calculated derivatives of the coexistence curve $\mu = \mu_{AFM}(\pi/2 - \theta)$ with respect to its argument (denoted as $\mu'_{AFM}$) for different values of line tension ($\tilde{\tau}_{1lg} = \tilde{\tau}_{2lg} = \tilde{\tau}$): (a) $\tilde{\tau} = -2h$, (b) $\tilde{\tau} = -h$, (c) $\tilde{\tau} = 0$, (d) $\tilde{\tau} = h$, (e) $\tilde{\tau} = 2h$ for specific choice of $\varphi = \pi/6$ and $\theta_1 = \theta_2 = \theta$. Dashed lines are drawn to guide the eye.

namely $\lambda = \sigma_{lg}/\Delta\mu\Delta\rho$. The equation for the coexistence line ($\Delta\Omega[\bar{f}] = 0$) can be rewritten as $\mathcal{F}_0\left(\theta, \varphi, \frac{\lambda}{h}\right) = 0$, where $\mathcal{F}_0$ is a dimensionless function. Thus the phase diagrams displayed in variables $\pi/2 - \theta$ and $\mu - \mu_0(T)$ measured in $\sigma_{lg}/\Delta\rho h$ do not depend any more on height $h$. If one considers a system with non-zero line tension then there is one additional parameter with the dimension of length, namely $\tilde{\tau}$. This time the equation for the coexistence curve takes the form $\mathcal{F}_\tau\left(\theta, \varphi, \frac{\lambda}{h}, \frac{\tilde{\tau}}{h}\right) = 0$ and the coexistence lines corresponding to different $h$-values are not identical unless $\tilde{\tau}$ is properly rescaled; see figure 8.

## 5. Sizes of liquid bridges

The significant aspect of the present analysis is that it is applicable to macroscopic objects. However, in figure 2 we see that the size of determined liquid bridges can vary substantially depending on the chosen values of the system's parameters. In this paragraph we analyze this issue in more detail, in particular from the perspective of the requirement that analyzed objects are macroscopic.

As the measure of the width $w$ of the bridge we take the minimal value of $\bar{f}(z)$ in the range $z = 0$ to $z_2$. For macroscopic bridges considered in this paper their width must be large compared to the bulk correlation length $\xi$, which we take to be in the nanometer range. In other words, *a posteriori* only parameter values should be taken into account such that the corresponding bridges are macroscopic, i.e. $w \geqslant \xi$. The way that the width $w$ depends on

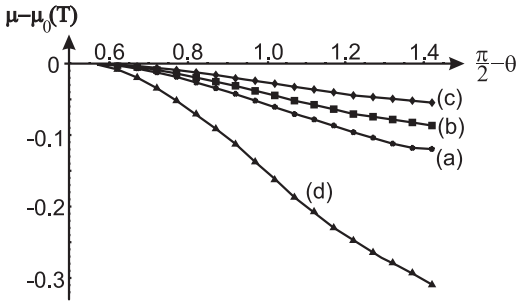


**Figure 8.** Numerically determined coexistence lines corresponding to a fixed value of line tension $\tilde{\tau} = 1$ au and for different values of height $h$: (a) $h = 1$ au, (b) $h = 2$ au, (c) $h = 3$ a.u. In the case of $\tilde{\tau} = 0$ the above coexistence lines corresponding to different $h$-values become identical; curve (d). The opening angle is fixed and equal to $\varphi = \pi/6$. The difference $\mu - \mu_0(T)$ is measured in $\sigma_{\mathrm{lg}}/h\Delta\rho$ units. Solid lines are drawn to guide the eye.

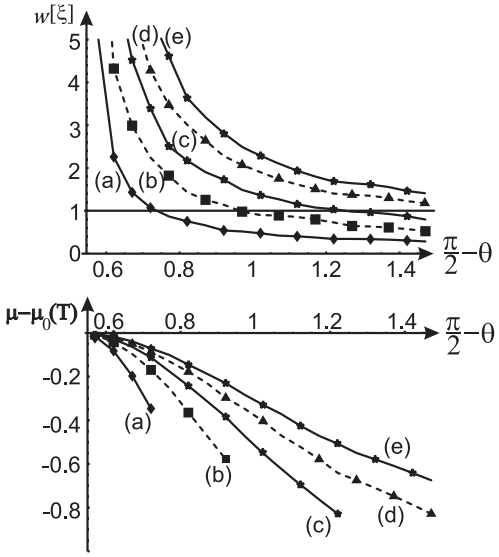


**Figure 9.** The bridge's width $w$ measured in $\xi$ units (upper graph) evaluated along the corresponding coexistence curves shown on the phase diagram (lower graph). The curves are displayed for a range of $\theta$ values at which a macroscopic approach corresponding to $w \geqslant 1$ is applicable—$h$-values: (a) $h = 0.1\xi$, (b) $h = 0.3\xi$, (c) $h = 0.5\xi$, (d) $h = 0.7\xi$, (e) $h = 0.9\xi$. The angle $\varphi = \pi/6$ and $\tau = 0$. The difference $\mu - \mu_0(T)$ is measured in $\sigma_{\mathrm{lg}}/\Delta\rho\xi$ units. Solid lines are drawn to guide the eye.

parameters $h$, $\varphi$, and $\tau$ are depicted in figures 9–11. For angles $\theta \leqslant \theta^*(\varphi)$ the width of the bridge grows to infinity upon approaching the bulk coexistence independent of the sign of $\tau$. On the other hand, for $\theta > \theta^*(\varphi)$ the width of the bridge achieves at bulk coexistence a finite value for negative $\tau$.

For small $h$-values and $\tilde{\tau} \approx 0.1\xi$ (for typical values of $\tau = 10^{-11}$ J m$^{-1}$ and $\sigma_{\mathrm{lg}} = 10^{-2}$ J m$^{-2}$, the coefficients $\tilde{\tau} = \tau/\sigma_{\mathrm{lg}}$ are in the nanometer range) our macroscopic analysis predicts for $\varphi$ close to $\pi/2$ the existence of bridges with a width smaller than $\xi$. One has to treat these results with caution because such a situation requires a more detailed approach than the present macroscopic description; see [47] for similar arguments in the case of wedge filling

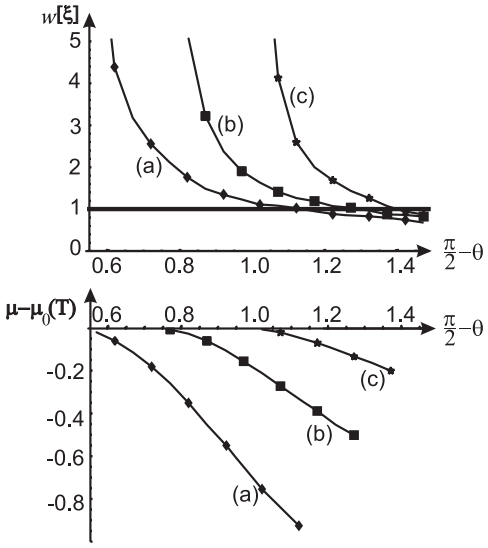


**Figure 10.** The bridge's width $w$ measured in $\xi$ units (upper graph) evaluated along the corresponding coexistence curves shown on the phase diagram (lower graph). The curves are displayed for a range of $\theta$ values at which macroscopic approach corresponding to $w \geqslant 1$ is applicable: (a) $\varphi = 0.5$, (b) $\varphi = 0.7$ and (c) $\varphi = 0.9$. The height $h = 0.25\xi$ and $\tau = 0$. The difference $\mu - \mu_0(T)$ is measured in $\sigma_{\mathrm{lg}}/\Delta\rho\xi$ units. Solid lines are drawn to guide the eye.

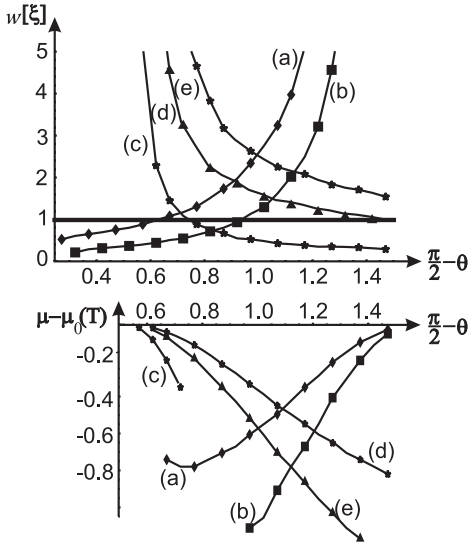


**Figure 11.** The bridge's width $w$ measured in $\xi$ units (upper graph) evaluated along the corresponding coexistence curves shown on the phase diagram (lower graph). The curves are displayed for a range of $\theta$ values at which macroscopic approach corresponding to $w \geqslant 1$ is applicable: (a) $\tilde{\tau} = -0.2\xi$, (b) $\tilde{\tau} = -0.1\xi$, (c) $\tilde{\tau} = 0$, (d) $\tilde{\tau} = 0.1\xi$, (e) $\tilde{\tau} = 0.2\xi$. The height $h = 0.1\xi$ and $\varphi = \pi/6$. The difference $\mu - \mu_0(T)$ is measured in $\sigma_{\mathrm{lg}}/\Delta\rho\xi$ units. Solid lines are drawn to guide the eye.

transitions. We note that the minimal size of the bridge included in our analysis cannot be smaller then the largest among the parameters $h$ and $|\tilde{\tau}|$ which have the dimension of length.

This restriction reduces the range of parameters for which reliable phase diagrams can be constructed within present approach.

## 6. Summary

We analyzed macroscopically the formation of liquid bridges in an AFM-like geometry in three dimensions with the microscope tip modeled by a cone. In the case when the line tension is not taken into account the properties of the phase diagram displaying the coexistence of two phases—one with the liquid bridge present and the other without bridge—is similar to the phase diagram obtained for the two-dimensional version of this problem. The coexistence line is an increasing function of the contact angle $\theta$, and it meets the bulk coexistence line tangentially at the value of the contact angle $\theta^*(\varphi)$ corresponding to the filling transition. We provide a numerically obtained plot of $\pi/2 - \theta^*$ versus $\varphi$ which points—at least for small $\varphi$ values—to a linear dependence with prefactor 1. We also note that the particular value $\theta^* = 0$ corresponding to wetting is obtained not for $\varphi = \pi/2$ but for smaller value $\varphi = \varphi_0 = 1.42$.

In the presence of non-zero line tension values, in particular negative ones, the shape of the coexistence line changes substantially. For negative values of line tension coefficients the coexistence lines exhibit local minima and reapproach the bulk coexistence ($\mu = \mu_0$) for small values of angle $\theta$ corresponding to temperatures close to $T_w$. In addition, we analyzed the size of the bridge present in the system and displayed its dependence on system parameters. Our investigations are limited to macroscopic bridges and to situations in which line tensions are treated as constants, i.e. do not depend on the thermodynamic state of the system. The requirement that the characteristic lengths of this problem are larger than the bulk correlation length reduces the range of parameters at which reliable conclusions can be drawn; this is depicted on figures 9–11.

The main objects of our analysis in this paper were the phase diagrams for fluid confined in AFM-like geometry with special emphasis on the structure of the coexistence curves along which the phase with the liquid bridge spanning the walls and the phase without such a bridge coexist. Unfortunately, there exist no experimental data which could be compared with our predictions. Most of the experimental and simulational data on such systems refer to the properties of the force between the AFM walls induced by the presence of the liquid bridge and not to the structure of the phase diagram itself. We find that it is important to have an overall view of the phase diagram before answering the more detailed questions referring to such systems, like the dependence of this force on the distance between the tip apex and the planar substrate, or the role of thermal fluctuations.

A more detailed analysis based on the effective capillary Hamiltonian [25, 26] might—in principle—allow one not only to determine the expressions for the relevant line tension coefficients (already mentioned in section 2) but also to help to estimate the role of fluctuations on the formation and stability of liquid bridges investigated in this paper. We point to difficulties related to the above mesoscopic formulation of the bridge formation problem.

## Acknowledgments

The authors express their gratitude to S Dietrich, P Jakubczyk, and A Majhofer for many helpful discussions. This work has been financed from funds provided for scientific research for years 2006–2008 under research project N202 076 31/0108.

## References

[1] Eijkel J C T and van den Berg A 2005 *Microfluid. Nanofluid.* **1** 249
[2] Squires T M and Quake S R 2005 *Rev. Mod. Phys.* **77** 977

[3] de Gennes P G 1985 *Rev. Mod. Phys.* **57** 827
[4] Evans R and Marconi M B 1987 *J. Chem. Phys.* **86** 15
[5] Parry A O and Evans R 1992 *Physica* A **181** 250
[6] Rastagno F, Bocquet L and Biben T 2000 *Phys. Rev. Lett.* **84** 2433
[7] Talanquer V and Oxtoby D W 2001 *J. Chem. Phys.* **114** 2793
[8] Rowlinson J S and Widom B 1989 *Molecular Theory of Capillarity* (Oxford: Clarendon)
[9] Andrienko D, Patricio P and Vinogradova O I 2003 *J. Chem. Phys.* **121** 4414
[10] Piner R D and Mirkin C A 1997 *Langmuir* **13** 6864
[11] Choe H *et al* 2005 *Phys. Rev. Lett.* **95** 187801
[12] Dobbs H T, Darbellay G A and Yeomans J M 1992 *Europhys. Lett.* **18** 439
[13] Lambert P and Delchambre A 2005 *Langmuir* **21** 9537
[14] Paramonov P B and Lyuksyutov S F 2005 *J. Chem. Phys.* **123** 084705
[15] Jang J, Schatz G C and Ratner M A 2004 *Phys. Rev. Lett.* **92** 885504
[16] Charlaix E and Crassous J 2005 *J. Chem. Phys.* **122** 184701
[17] Bowles A P *et al* 2006 *Langmuir* **22** 11436
[18] Crassous J, Charlaix E, Gayvallet H and Loubet J L 1993 *Langmuir* **9** 1995
[19] Farschchi-Tabrizi M *et al* 2006 *Langmuir* **22** 2171
[20] Lubarsky G V, Davidson M R and Bradley R H 2006 *Phys. Chem. Chem. Phys.* **8** 2525
[21] Jang J, Schatz G C and Ratner M A 2002 *J. Chem. Phys.* **116** 3875
[22] Piner R D *et al* 1999 *Science* **283** 661
[23] Schwartz P V 2002 *Langmuir* **18** 4041
[24] Vettiger P *et al* 2000 *IBM J. Res. Dev.* **44** 323
[25] Rejmer K, Dietrich S and Napiórkowski M 1999 *Phys. Rev.* E **60** 4027
[26] Jakubczyk P and Napiórkowski M 2002 *Phys. Rev.* E **66** 041107
[27] Dutka F and Napiórkowski M 2006 *J. Chem. Phys.* **124** 121101
[28] de Lazzer A, Dreyer M and Rath H J 1999 *Langmuir* **15** 4551
[29] Kralchevsky P A and Denkov N D 2001 *Curr. Opin. Colloid. Interface. Sci.* **6** 383
[30] Koiso M and Palmer B 2005 *Indiana Univ. Math. J.* **54** 1817
[31] Swain P S and Lipowsky R 1998 *Langmuir* **14** 6772
[32] Press W H *et al* 1992 *Numerical Recipes in C: The Art of Scientific Computation* 2nd edn (Cambridge: Cambridge University Press)
[33] Dietrich S 1988 *Phase Transitions and Critical Phenomena* ed C Domb and J L Lebowitz (New York: Academic)
[34] Schick M 1988 *Introduction to Wetting Phenomena* (*Les Houches Session* vol XLVIII)
[35] Evans R 1979 *Adv. Phys.* **28** 143
[36] Dietrich S and Napiórkowski M 1991 *Phys. Rev.* A **43** 1861
[37] Mecke K and Dietrich S 1999 *Phys. Rev.* E **59** 6766
[38] Napiórkowski M, Koch W and Dietrich S 1992 *Phys. Rev.* A **45** 5760
[39] Getta T and Dietrich S 1998 *Phys. Rev.* E **57** 655
[40] Jakubczyk P and Napiórkowski M 2004 *J. Phys.: Condens. Matter* **16** 6917
[41] Jakubczyk P and Napiórkowski M 2005 *Phys. Rev.* E **72** 011603
[42] Pompe T and Herminghaus S 2000 *Phys. Rev. Lett.* **85** 1930
[43] de Gennes P G, Brochard-Wyart F and Quere D 2004 *Capillary and Wetting Phenomena: Drops Bubbles Pearls Waves* (New York: Springer)
[44] Indekeu J O 1992 *Physica* A **183** 439
[45] Indekeu J O 1994 *Int J. Mod. Phys.* B **8** 309
[46] Wang J Y, Betelu S and Law B M 2001 *Phys. Rev.* E **63** 031601
[47] Hauge E H 1992 *Phys. Rev.* A **46** 4994